# Ultra-High Resolution Gamma-Ray Spectrometer Development for Nuclear Attribution and Non-Proliferation Applications

Stephane F. Terracol, Shafinaz Ali, Thomas R. Niedermayr, I. Dragos Hau, Owen B. Drury, Zaheer A. Ali, Toshiyuki Miyazaki, Mark F. Cunningham, Jonathan G. Dreyer, John D. Leacock, and Stephan Friedrich

***Abstract*—Cryogenic Gamma-ray spectrometers based on superconducting thermistors provide more than an order of magnitude improvement in energy resolution over conventional high-purity germanium detectors. They are based on measuring the temperature increase upon Gamma-ray absorption with a sensor operated at the transition between its superconducting and normal state. We are developing Gamma-ray calorimeters using Mo/Cu multilayer sensors with an attached Sn absorber for increased absorption efficiency ("UltraSpec"). We have also developed two-stage adiabatic demagnetization refrigerators for user-friendly detector operation at the required temperatures of ~0.1 K. The spectrometer has achieved an energy resolution between 50 and 90 eV FWHM for photon energies up to 100 keV, and can be operated up to 0.4 MeV with reduced resolution. We present an update on spectrometer performance and sensitivity, and discuss the relevance of this technology for Gamma-ray analysis in nuclear attribution and nuclear non-proliferation applications.**

## I. Introduction

Gamma (γ) spectrometry is widely used to determine the isotopic composition of radioactive materials [1]. Upon decay, each radioisotope emits γ-rays with characteristic energies, which provide a fingerprint of the sample's composition. Relative line intensities can then be used to determine isotope ratios and infer sample age, origin and processing history. Traditionally, high-purity germanium (HPGe) detectors operating at liquid nitrogen temperatures of $T \approx 77$ K have been used for γ-ray analysis, since they combine high energy resolution needed to separate the emission from different isotopes with high absorption efficiency required to measure weak emission lines from dilute samples. HPGe detectors enable isotope ratio measurements with an error of ~1% or better depending on the sample, limited either by counting statistics or by systematic errors in detection efficiency or background subtraction. Precision measurements for nuclear attribution or non-proliferation applications therefore rely on the analysis of intense γ-lines with similar energies, so that statistical errors are small and detection efficiencies are similar. These lines typically fall in the range between ~50 and ~200 keV, and are often affected by spectral interferences. Since the attribution of unknown nuclear samples or the exposure of illegal activities often relies on measuring minute differences in isotopic composition, high-resolution spectrometers are essential for nuclear forensics.

Cryogenic γ-ray spectrometers operating at temperatures of $T \approx 0.1$ K offer an order of magnitude improvement in energy resolution over conventional high-purity Ge (HPGe) detectors [2]. They consist of an absorber with heat capacity $C$ and a sensitive thermometer, both weakly thermally linked to a cold bath (figure 1, inset). A γ-ray with energy $E_\gamma$ will increase the absorber temperature by an amount $E_\gamma/C$ proportional to the γ-ray energy, which can be measured with the attached thermometer before both absorber and thermometer cool back down to the bath temperature through the weak thermal link. The energy resolution $\Delta E_{FWHM}$ of cryogenic spectrometers is fundamentally limited only by thermodynamic fluctuations, and can be well below 100 eV FWHM for operation at $T \approx 0.1$ K [3]-[5].

The Advanced Detector Group at Lawrence Livermore National Laboratory is developing cryogenic γ-ray detectors based on bulk superconducting Sn absorbers coupled to sensitive Mo/Cu superconducting-to-normal transition edge sensors (TESs) for nuclear forensics (figure 1) [4]-[6]. We are also developing refrigeration and readout technology for user-friendly detector operation at ~0.1 K. These spectrometers have achieved an energy resolution between ~50 and 90 eV FWHM for energies below 100 keV, and are thus ideally suited for precise non-destructive analysis of nuclear samples. Here we discuss the spectrometer design and sensitivity, compare its performance with conventional semiconductor detectors for the analysis of uranium samples, and discuss their advantages for nuclear non-proliferation applications.

Manuscript received October 20, 2004. We gratefully acknowledge the financial support of the U.S. Department of Energy, Office of Non-Proliferation Research and Engineering, NA-22. This work was performed under the auspices of the U.S. Department of Energy by University of California Lawrence Livermore National Laboratory under contract No. W-7405-Eng-48.

S. F. Terracol, S. Ali, T. R. Niedermayr, I. D. Hau, O. B. Drury, Z. A. Ali, T. Miyazaki*, M. F. Cunningham*, J. G. Dreyer*, J. D. Leacock* and S. Friedrich are (or *were) with the Advanced Detector Group at the Lawrence Livermore National Laboratory, L-270, Livermore, CA 94550, U.S.A. (telephone: +1-925-423-1527, fax: +1-925-424-5512, e-mail: friedrich1@llnl.gov).

## II. Theoretical Considerations

### A. Composite Transition Edge Sensors

Cryogenic γ-ray calorimeters consist of a bulk absorber with heat capacity $C_{abs}$ attached to a TES thermistor, both of which are weakly coupled to a cold bath through a thermal conductance $G$ (figure 1). In the simplest case [3], thermodynamic energy fluctuations $4k_BT^2G$ across this thermal conductance limit the energy resolution to

$$\Delta E_{FWHM} \approx 2.355\sqrt{k_B T^2 C}. \quad (1)$$

This limit arises from the random passage of phonons, each of which carries an average energy $\sim k_BT$, between the absorber and the cold bath across the weak thermal link. An absorber at temperature $T$ contains a total energy $\sim CT$, and thus a number of phonons $\sim CT/k_BT = C/k_B$. Assuming Poisson's statistics, this number of phonons will fluctuate by $\sqrt{(C/k_B)}$, causing rms energy fluctuations of $\sqrt{(k_BT^2C)}$.

Attaching a bulk absorber to the TES thermistor increases the detection efficiency, but deteriorates the limiting resolution, since both the thermal conductances from the glue between the absorber and the TES ($G_{abs}$), and from the membrane between the TES and the cold bath ($G_{TES}$) contribute fluctuations $k_BT^2G$ to the total noise. On the other hand, the finite conductance serves as a thermal bottleneck and thereby reduces spatial variation in the detector response. Preamplifier noise and Johnson noise can be kept sufficiently low to not affect the energy resolution.

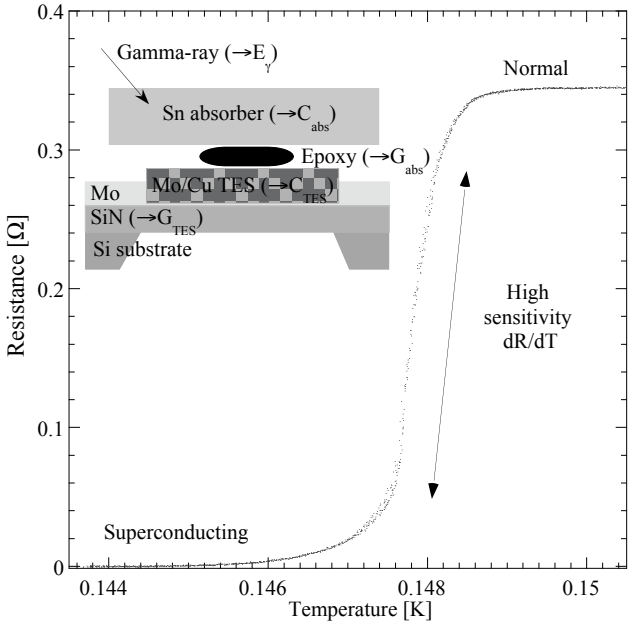


Fig. 1. Resistive transition between the superconducting and the normal state of a Mo/Cu multilayer transition edge sensor (TES). Detector operation in the steep part of the transition ensures high sensitivity. The inset shows a schematic design of a single TES detector pixel, consisting of a superconducting Mo/Cu sensor and an attached bulk Sn absorber, both weakly coupled to a cold Si substrate through a thin SiN membrane.

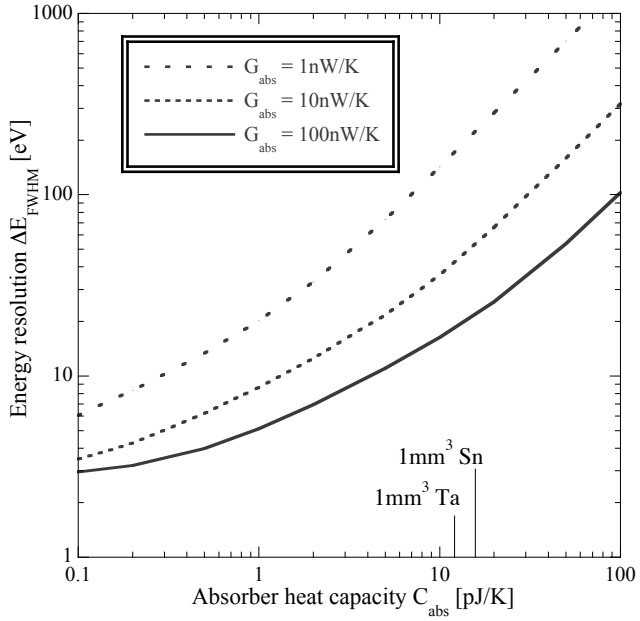


Fig. 2. Theoretical energy resolution at $T = 0.1$ K as a function of absorber heat capacity $C_{abs}$, i.e. absorber volume, for different degrees of thermal coupling $G_{abs}$ between the absorber and the TES sensor. The graph illustrates the trade-offs in detector design between highest energy resolution and absorption efficiency.

### B. Energy Resolution

To simulate the response of a composite TES calorimeter we exploit the analogy between thermal and electric circuits ($T \Leftrightarrow V$, $P \Leftrightarrow I$, $C_{th} \Leftrightarrow C_{el}$, $G_{th} \Leftrightarrow 1/R_{el}$) and calculate the response using commercially available SPICE circuit simulation routines [5], [7], [8]. For most of the signal band of a few kHz, the noise is dominated by fluctuations $k_BT^2G_{abs}$ between absorber and TES. Only at frequencies below $G_{abs}/2\pi C_{abs}$ this noise contribution is reduced, because the absorber cannot change its temperature relative to TES and thus benefits from electrothermal feedback (ETF) [9]. Johnson noise $4k_BT/R_{TES}$ only contributes at very high frequencies and is negligible.

The energy resolution for different detector designs can be calculated by integrating the simulated spectral noise density over the appropriate optimum filter bandwidth (figure 2) [3], [5]. As expected from equation (1), the noise for composite microcalorimeters increases with increasing absorber heat capacity and thus absorber volume. The detector resolution improves with increasing thermal coupling $G_{abs}$ between absorber and TES, since it increases the frequency range over which ETF reduces the dominant noise source (figure 2). One therefore faces a trade-off between energy resolution and absorption efficiency, with the overall performance improving with increasing $G_{abs}$. For typical values of $G_{abs}$ in the 10 nW/K range for the ~200 μm diameter ~25 μm thick epoxy dots used in our detector design, a desirable energy resolution below 100 eV FWHM limits the size of an absorber pixel to ~mm$^3$ at $T \approx 0.1$ K.

### C. Sensitivity

To quantify the sensitivity of cryogenic detectors for isotope ratio measurements, we consider the general case of two emission lines at known energies $E_1$ and $E_2$ with a total number of counts $N_1$ and $N_2$ on a background $B$ (figure 3, inset). We assume that the lineshape is Gaussian and set by the energy resolution $\Delta E_{FWHM}$ of the spectrometer. This assumption is an acceptable approximation to observed response functions, although it ignores the effects of incomplete charge collection in HPGe detectors and lifetime-broadened X-ray lines in cryogenic spectrometers. For two overlapping lines on a constant (Compton) background, the errors $\sigma_1$ and $\sigma_2$ for measuring the intensities $N_1$ and $N_2$ can be calculated analytically [10], yielding

$$\sigma_1^2 = aB + bN_1 + cN_2$$
$$\sigma_2^2 = aB + bN_2 + cN_1 \qquad (2)$$
$$\text{with } a = \frac{\Delta E_{FWHM}\sqrt{\pi}}{\sqrt{2\ln 2}(1-d^2)},\ b = \frac{2-4d^{7/3}+2d^{10/3}}{\sqrt{3}(1-d^2)^2},$$
$$c = \frac{2d^{4/3}-4d^{7/3}+2d^2}{\sqrt{3}(1-d^2)^2},\ d = e^{-2\ln 2(E_1-E_2)^2/\Delta E_{FWHM}^2}.$$

Equation (2) describes the statistical precision in the limiting case that systematic errors are negligible. It quantifies this limit in terms of line separation $E_1$ - $E_2$ and detector resolution $\Delta E_{FWHM}$, which enter through the parameters $d$ and a. The parameter $a$ describes the influence of the background $B$ on the precision, and correctly leads to $\sigma_{1,2} \propto \sqrt{\Delta E_{FWHM}}$ when background statistics dominate the spectrum, i.e. in the limit $d \rightarrow 0$ and $B >> (N_1 + N_1)$. The parameter $c$ quantifies the influence of the overlap of one line on the precision for measuring the other line. As expected, $c \rightarrow 0$ for well separated lines, i. e. $d \rightarrow 0$ for $(E_1 - E_2) >> \Delta E_{FWHM}$.

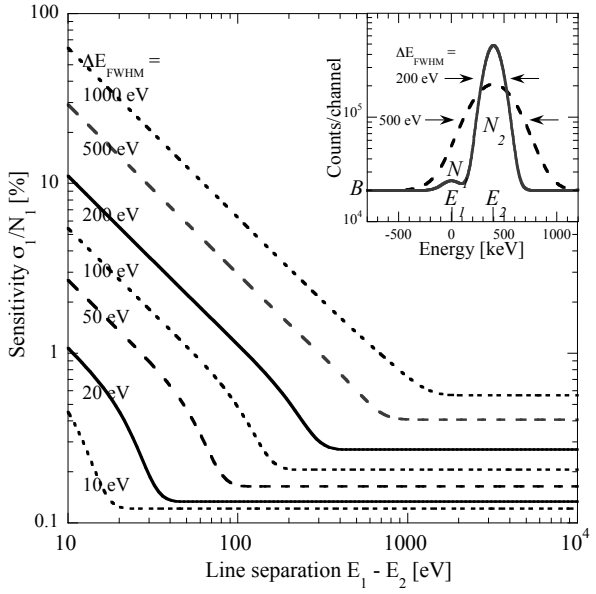


Fig. 3. Spectrometer sensitivity as a function of line separation $E_1$ - $E_2$ for different resolution $\Delta E_{FWHM}$. according to equation (2) for $N_1 = 10^6$ and $N_2 = 10^8$ counts. The inset shows two lines with an intensity ratio $N_1$:$N_2$ = 1:100 separated by $E_1$ - $E_2$ = 400eV on a constant background $B$ for a spectrometer resolution of 200 and 500 eV.

Figure 3 quantifies the improvements in sensitivity that high energy resolution provides in the case of two lines with an intensity ratio of 1:100 on a constant background as a function of line separation [11]. For two lines separated by $(E_1 - E_2)$, an energy resolution $\Delta E_{FWHM} = (E_1 - E_2)/2$ is generally sufficient to fully remove line overlap, even in the case of extreme intensity ratios. Further improvements in energy resolution increase the sensitivity only in proportion to $\sqrt{\Delta E_{FWHM}}$, because the influence of the spectral background $B$ is reduced.

For uranium and plutonium, the materials most relevant in the context of nuclear non-proliferation, emission lines used for precision isotopic analysis are separated by ~100 to ~500 eV. We therefore design our cryogenic spectrometers for an energy resolution between ~50 and ~200 eV, in order to reduce the limiting error for nuclear isotopics by an order of magnitude compared to conventional HPGe detectors.

### D. Systematic errors

The preceeding analysis based on (2) considers only *statistical* limitations of isotope analysis by γ–spectroscopy, and therefore constitutes an upper limit to the precision. In most practical analyses, *systematic* errors reduce the accuracy below that limit. This is because the expression

$$\frac{\text{isotope 1}}{\text{isotope 2}} = \frac{N_1}{N_2}\cdot\frac{\xi_2}{\xi_1}\cdot\frac{\eta_2}{\eta_1} \qquad (3)$$

describes the isotope ratio with statistics-limited precision only if branching ratios (γ–ray yields) $\xi_2/\xi_1$ and γ–detection efficiencies $\eta_2/\eta_1$ are known with at least the same precision as the line intensities $N_1$ and $N_2$. This is, in general, not the case. There are three contributions to the systematic error:

- The dominant systematic error arises from variations in γ-detection efficiency $\eta = \eta_{det}\tau_{shield}\eta_{self}$. For once, the detector absorption efficiency $\eta_{det}$ and the shielding transmission $\tau_{shield}$ vary with energy and measurement geometry, but -more fundamentally- the sample itself re-absorbs a certain fraction of the radioactivity. Since the exact sample composition is usually unknown, the variations in self-absorption $\eta_{self}$ introduce a fundamental error that cannot be eliminated a priori by careful detector calibration. This can be addressed by using γ-lines with similar energy for which the detection efficiency $\eta$ is similar [1, 12]. In addition, the efficiency can be locally calibrated for each spectrum by comparing the measured intensities of emissions from the same isotope for which the relative γ-yields are known. Cryogenic detectors can reduce the systematic error due to $\eta(E)$ since they allow

analyses and efficiency corrections on more closely spaced lines without increasing the errors from line overlap.

- A second systematic error arises from uncertainties in the spectral background, which can, in general, not be assumed as constant. Nuclear isotopic analysis often relies on algorithms to derive the background over a range several keV, based on its average value, the line shapes in that range and its slope at the edges [12]. If we estimate that the contribution of this error is reduced in proportion to the energy range of the background approximation, we can expect a reduction by a factor of ~7 for Pu and ~4 for U isotope analysis when using cryogenic detectors.
- Ultimately, the limiting systematic error arises from the uncertainty of the branching ratios $\zeta$. Typically, $\zeta$ is known to between ~0.05 and ~1%, its precision being limited mostly by uncertainties in absolute detection efficiency in the experiments designed to measure them. This error is largely unaffected by improvements in energy resolution, and will eventually limit the accuracy of many isotope ratio measurements by γ-spectroscopy.

Still, we estimate an overall reduction in systematic errors by an order of magnitude when using cryogenic detectors [11].

## III. Experimental Results

### A. Spectrometer design

For user-friendly Gamma-ray analysis with TES calorimeters we have built a spectrometer that holds the detector at ~0.1 K at the end of a cold finger within ~2 cm of a radioactive sample at room temperature (figure 4). The spectrometer uses a nested design, with liquid nitrogen and liquid helium tanks for pre-cooling to 77 K and 4.2 K, respectively, and a two-stage adiabatic demagnetization refrigerator (ADR) to attain a base temperature of ~70 mK. Adiabatic demagnetization is the process of cooling below a liquid He bath temperature by isothermal magnetization and adiabatic demagnetization of a paramagnetic material. Our spectrometer uses two different paramagnets on two separate stages to allow operation with an unpumped liquid He bath at a temperature of 4.2 K

Fig. 4. Superconducting spectrometer ("UltraSpec"). γ-rays from the radioactive source on the left are detected by the TES detector held at ~0.1 K at the end of the cold finger. The signals are amplified at 4.2 K, readout with electronics in the enclosure on the right, and digitally processed.

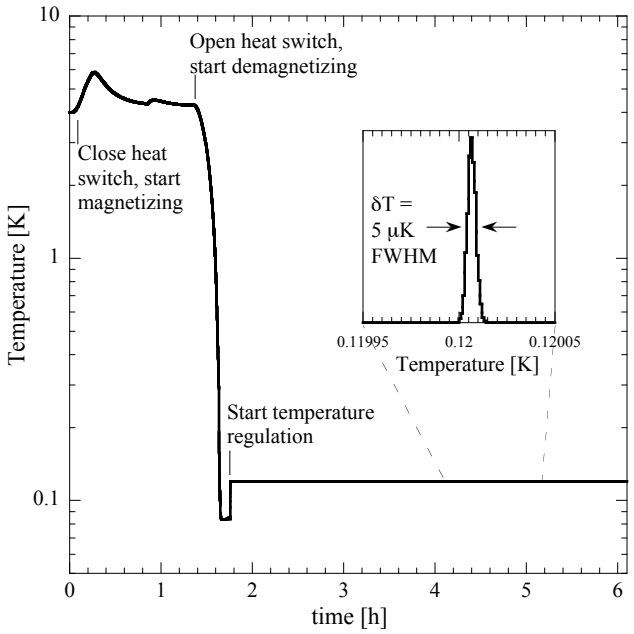


Fig. 5. Temperature evolution T(t) during a demagnetization cycle. During magnetization, T rises above the 4.2 K He bath temperature because of the finite thermal conductance of the heat switch. After demagnetization, T is regulated at 0.12 K. The inset shows a histogram of the temperature readings over a typical one-hour period.

[13],[14]. The first (guard) stage is cooled by a gadolinium gallium garnet $Gd_3Ga_5O_{12}$ (GGG) to a temperature of ~1 K, and the second (detector) stage is cooled to a base temperature of ~70 mK by a $Fe(NH_4)(SO_4)_2 \times 12\ H_20$ salt pill, commonly known as FAA for ferric ammonium alum. During the cooling cycle, the paramagnets are first magnetized in a ~4 T magnetic field controlled with a Delta Elektronika SM1540D power supply, while the heat of magnetization is carried into the He bath through a closed custom-designed electro-mechanical heat switch [14]. After equilibration at 4.2 K, the heat switch is opened to thermally decouple the paramagnets, and the base temperature is attained by adiabatically reducing the magnetic field. The cycle is automated using a USB-interfaced Labview PID controller, takes about ~1 h, and allows detector operation for ~8 to ~20 h between cycles depending on the heat load into the cold stage and the operating temperature of the detector (figure 5). During operation, the detector stage temperature can be kept stable to ±5 μK FWHM by controlling the residual magnet current with a low noise Agilent 3640A power supply (figure 5, inset), limited by the sensitivity $\partial R/\partial T = 38\ \Omega/mK$ of the cold stage thermometer and by the ~0.1 Ω rms error of the Picowatt AVS-47 resistance bridge of the temperature readout.

The TES detector is mounted at the end of a Au-plated oxygen-free high-conductivity Cu cold finger, which is surrounded by a liquid-He-cooled and a liquid-$N_2$-cooled radiation shield, and μ-metal magnetic shielding at room temperature. ADRs are compact, reliable and easy to use.

### B. *Spectrometer Performance*

We have characterized TES γ–ray detectors with different absorber sizes and examined the trade-offs between energy resolution, detection efficiency and dynamic range. In all cases, the TES thermistor consists of a superconducting 0.5 × 0.5 $mm^2$ Mo/Cu multilayer, and is operated in the ADR cryostat with the bath temperature regulated to ~100 mK. The detector is voltage biased at the onset of the transition and exposed to radiation. The current signal is amplified with a superconducting quantum interference device (SQUID) preamplifier at 4.2 K in a flux-locked loop with a gain of 14, and a custom-designed room temperature amplifier with an input voltage noise of ~1 nV/√Hz. The full waveforms are captured, optimally filtered off-line and histogrammed.

Figure 6 shows the response of a detector with a small 1 × 1 × 0.25 $mm^3$ Sn absorber to a $^{241}$Am and a $^{57}$Co calibration source. The resolution is 52 eV FWHM at 60 keV, roughly consistent with figure 2 for a thermal conductance $G_{abs} \approx 10$ nW/K. It degrades slightly to 73 eV at 122 keV, most likely due to small spatial variations in the detector response. This resolution is more than sufficient to fully separate all γ and X-ray emission lines below 120 keV that are relevant for U and Pu isotopics.

In fact, for many nuclear non-proliferation applications it is desirable to trade off some energy resolution for increased efficiency. One such case is shown in figure 7, where a TES with a larger 2 × 2 × 0.25 $mm^3$ Sn absorber has been exposed to radiation from typical natural uranium concentrate used as a starting product for uranium processing ("yellowcake"). It contains 99.28% $^{238}$U and 0.72% $^{235}$U. Most of the visible lines below 200 keV originate from $^{235}$U, $^{234}$Th and X-ray fluorescence (table 1), and are well separated by commercial HPGe spectrometers (figure 7, top).

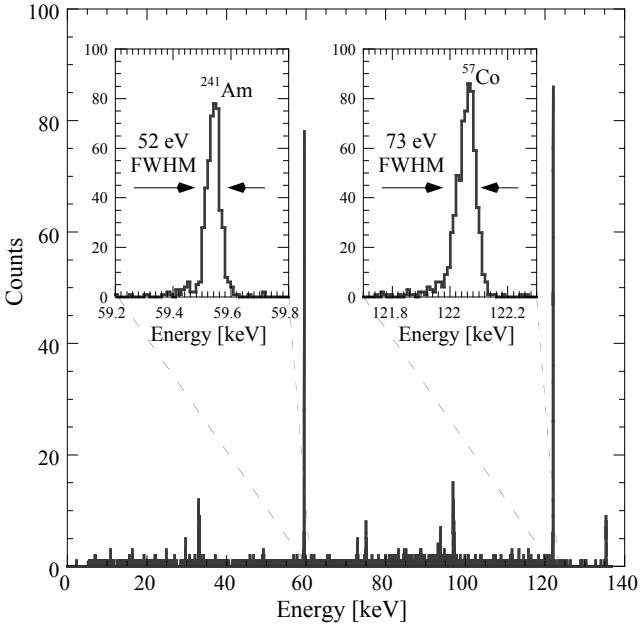


Fig. 6. High-resolution γ-spectrum of a calibration source using a Mo/Cu TES with a small 1 × 1 × 0.25 $mm^3$ Sn absorber.

TABLE 1: STRONGEST LOW ENERGY EMISSION LINES FROM NATURAL URANIUM AND ITS INITIAL DAUGHTER NUCLEI

| Nucleus | E [keV] | Line | Branching Ratio [%] |
|---|---|---|---|
| $^{238}$U | 49.55 | γ | 0.064 |
| $\tau_{1/2}$ = 4.47Gy | 89.957 | Th $K_{\alpha 2}$ | 0.017 |
| | 93.350 | Th $K_{\alpha 1}$ | 0.03 |
| $^{234}$Th | 63.29 | γ | 4.8 |
| $\tau_{1/2}$ = 24.1d | 92.38 | γ | 2.81 |
| | 92.80 | γ | 2.77 |
| $^{234}$Pa | 94.654 | U $K_{\alpha 2}$ | 14.4 * |
| $\tau_{1/2}$ = 6.70h | 98.434 | U $K_{\alpha 1}$ | 23.3 * |
| | 99.853 | γ | 3.2 |
| | 110.421 | U $K_{\beta 3}$ | 2.87 * |
| | 111.298 | U $K_{\beta 1}$ | 5.44 * |
| | 111.964 | U $K_{\beta 5}$ | 0.201 * |
| | 114.445 | U $K_{\beta 2}$ | 2.10 * |
| | 114.844 | U $K_{\beta 4}$ | 0.75 * |
| | 111.964 | U $K_{\beta 5}$ | 0.201 * |
| | 114.445 | U $K_{\beta 2}$ | 2.10 * |
| | 114.844 | U $K_{\beta 4}$ | 0.75 * |
| | 131.30 | γ | 18 |
| | 152.720 | γ | 6.0 |
| $^{234}$U | 53.20 | γ | 0.123 |
| $\tau_{1/2}$ = 245ky | 93.350 | Th $K_{\alpha 1}$ | 0.004 |
| $^{230}$Th | 67.67 | γ | 0.377 |
| $\tau_{1/2}$ = 75.4ky | 88.471 | Ra $K_{\alpha 1}$ | 0.0071 |
| $^{226}$Ra | 81.069 | Rn $K_{\alpha 2}$ | 0.192 |
| $\tau_{1/2}$ = 1.60ky | 83.787 | Rn $K_{\alpha 1}$ | 0.319 |
| | 186.211 | γ | 3.59 |
| $^{235}$U | 89.957 | Th $K_{\alpha 1}$ | 6 |
| $\tau_{1/2}$ = 704My | 93.350 | Th $K_{\alpha 2}$ | 11 |
| | 104.819 | Th $K_{\beta 3}$ | 1.3 |
| | 105.604 | Th $K_{\beta 1}$ | 2.4 |
| | 108.583 | Th $K_{\beta 2}$ | 0.9 |
| | 108.955 | Th $K_{\beta 4}$ | 0.33 |
| | 109.16 | γ | 1.54 |
| | 140.76 | γ | 0.22 |
| | 143.764 | γ | 10.96 |
| | 163.358 | γ | 5.08 |
| | 185.712 | γ | 57.2 |
| | 194.94 | γ | 0.63 |
| $^{231}$Th | 81.227 | γ | 0.89 |
| $\tau_{1/2}$ = 25.5 h | 84.216 | γ | 6.6 |
| | 89.944 | γ | 0.94 |
| | 92.282 | Pa $K_{\alpha 2}$ | 0.42 |
| | 95.863 | Pa $K_{\alpha 1}$ | 0.69 |
| $^{231}$Pa | 46.36 | γ | 0.223 |
| $\tau_{1/2}$ = 33.8ky | 87.675 | Ac $K_{\alpha 2}$ | 0.785 |
| | 90.886 | Ac $K_{\alpha 1}$ | 1.28 |
| $^{227}$Ac | 86.106 | Fr $K_{\alpha 1}$ | 0.015 |
| $\tau_{1/2}$ = 21.8y | 100.0 | γ | 0.009 |

* Since these lines can also be due to secondary excitation, their intensity depends on the uranium concentration in the sample.

However, two notable exceptions can only be fully resolved with cryogenic detectors, namely the $^{234}$Th/ Th $K_{\alpha 2}$ lines at ~92 keV and the $^{235}$U/ $^{226}$Ra emissions at ~186 keV. These lines play important roles in nuclear forensics for precision measurements of uranium enrichment and for monitoring uranium mining activities. A TES detector resolution of ~200 eV is perfectly adequate to completely resolve them (figure 7, bottom).

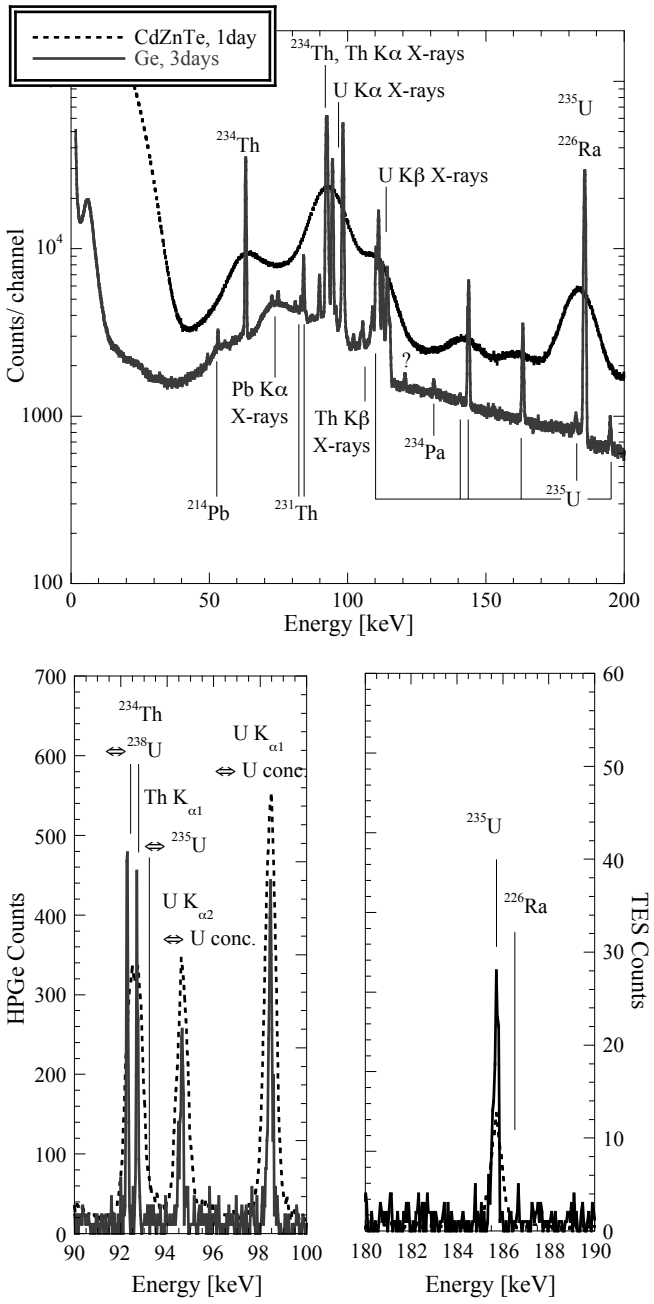


Fig. 7. Top: Low-energy region of the γ-spectrum for the uranium yellowcake sample, measured with commercial Ge and a CdZnTe detectors. Bottom: The emission lines in the 92 keV region and the 186 keV region can be fully resolved with cryogenic detectors (solid lines), but not with HPGe detectors (dashed lines).

Cryogenic detector design for operation at energies above ~200 keV is possible using even larger absorbers, with the attendant loss in energy resolution (figure 8). However, the performance of Ge or even CdZnTe detectors is usually sufficient above ~200 keV, making the case for cryogenic detectors less compelling for that energy range. In addition, high-energy γ-rays can drive the TES thermometer off the superconducting transition into the normal state where they are no longer sensitive, or at least drive it off the linear part

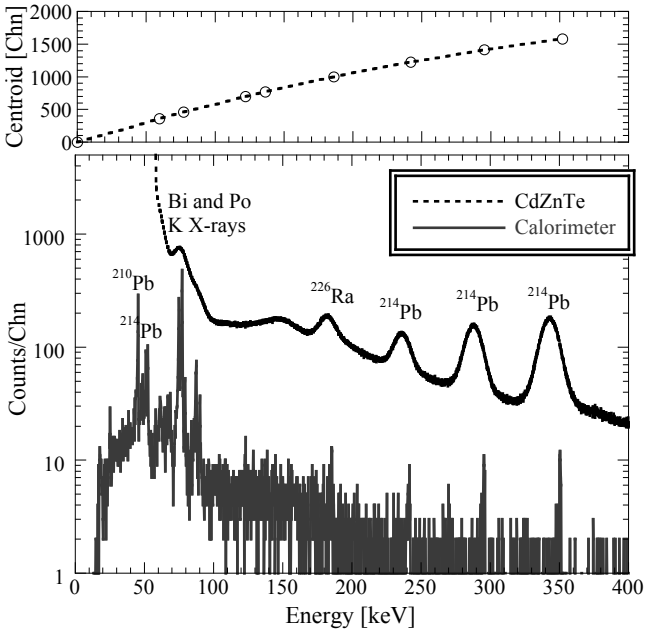


Fig. 8. Gamma spectra from a $^{226}$Ra source, demonstrating that cryogenic detector operation at energies above 200 keV is possible, albeit at reduced resolution and with low efficiency. The calibration curve (top) shows that the spectrometer response starts to become non-linear above ~200 keV as the detector bias moves off the linear part of the superconducting transition during a pulse (cf. Fig. 1).

of the transition (cf. figure 1). This causes the TES response to become non-linear at high energies (figure 8, top). We therefore typically optimize the TES performance for the energy range of 0 to ~200 keV, and use conventional semiconductor detectors at higher energies.

## IV. Discussion

In uranium isotopics, there are three areas where ultra-high energy resolution benefits nuclear non-proliferation work which have provided some of the initial driving force behind cryogenic detector technology development.

The first centers on precision measurements of uranium enrichment. While standard measurements of enrichment rely on measuring the magnitude of the 186 keV line from $^{235}$U above the Compton background, which can be done even with NaI scintillators, high-precision measurements are based on the $^{234}$Th lines at 92.38 and 92.80 keV as a measure of the $^{238}$U abundance, and the Th $K_{\alpha 1}$ X-ray at 93.35 keV as a measure of the $^{235}$U abundance [1, 15]. This analysis relies on the fact that the strong 186 keV Gamma emission from $^{235}$U excites X-rays from the Th daughter of U much more efficiently ($K_{\alpha 1}$-yield = 11%) than radiation released in the decay of $^{238}$U ($K_{\alpha 1}$-yield = 0.03 %). Note that these lines provide a measure of enrichment accurate to 0.1% only in samples at least ~170 days old because they require an equilibrium between the $^{234}$Th daughter ($\tau_{1/2}$ = 24 days) and the $^{238}$U parent, but they are still preferred for analysis because of their spectral proximity [1]. In addition, the U $K_{\alpha 1}$ and U $K_{\alpha 2}$ electronic X-ray transitions provide a measure of

the overall uranium concentration, since the α and γ-rays from the uranium decay are more likely to produce U X-rays in the presence of other U atoms near the location of the decay [15]. Furthermore, the relative fluorescence yield of the U $K_{\alpha 1}$ and U $K_{\alpha 2}$ lines are known, so that their measured spectral intensity provides a local calibration of the efficiency curve. Still, it is interesting that the analysis of the 92 keV region is the most precise non-destructive procedure to measure U enrichment, despite the overlap of the Th $K_{\alpha 1}$ X-ray line at 93.35 keV and the $^{234}$Th γ-emission at 92.80 keV when using HPGe detectors. This is because $^{238}$U has no strong low energy γ-emission lines that are close to any of the $^{235}$U emissions (table 1).

Cryogenic spectrometers that can fully separate these lines will further enhance this precision by reducing both statistical and systematic errors. The *statistical* error will be reduced since the two $^{234}$Th γ-rays and the Th $K_{\alpha 1}$ X-ray are separated by only 420 and 530 eV, and thus close to the limit where enrichment can be measured with HPGe detectors with an accuracy required for nuclear attribution (figure 3). In fact, measurements with Ge detectors routinely have an accuracy well below 1% *if* the enrichment level is intermediate and the intensity ratio of the $^{234}$Th and the Th $K_{\alpha 1}$ lines is not too far from unity. Unfortunately, the cases relevant in the context of nuclear non-proliferation are often those of very low or very high levels of enrichment, where the Th $K_{\alpha 1}$ : $^{234}$Th intensity ratio can be as high as several 100. Measurements close to the natural $^{235}$U concentration of 0.72% are important to assess if any $^{235}$U extraction has taken place at all, say in laboratories of nations with nuclear ambitions. Precision measurements of highly-enriched uranium are important to determine capabilities of enrichment processes and thus the potential of its producers to develop nuclear weapons.

Cryogenic detectors will also reduce *systematic* errors to measure U enrichment, since they allow using the $^{234}$Th lines at 92.38 and 92.80 keV for local efficiency corrections, rather than relying on the U $K_{\alpha}$ lines at 94.654 and 98.434 keV. In addition, the errors for the photon yields of the γ-ray and X-ray lines involved can be significantly reduced, and the background be subtracted more precisely when the lines are fully separated. This should reduce systematic errors by an order of magnitude and increase the accuracy of the measurement accordingly, even in cases of extreme levels of enrichment.

A second area of interest for using cryogenic high-resolution Gamma-spectrometers in the area of nuclear safeguards is for the detection of illegal uranium mining activities [16, 17]. Under geological conditions, there is a well-defined secular decay equilibrium ratio between uranium and its daughter products. The associated equilibrium ratio of the nuclear emission lines is disturbed if any mining activities have taken place. High-precision measurements of this ratio in often very dilute ores or tailings again require strong lines with similar energies to reduce the need for efficiency corrections. The $^{235}$U γ-emission at 185.712 keV and the line at 186.211 from the $^{238}$U daughter $^{226}$Ra emission are ideally suited for this purpose (table 1). Their ratio is ~1:21 in secular equilibrium, lower in the uranium products, and significantly higher in the tailings. However, the two lines are very close in energy, and the precision is affected by line-overlap when using HPGe detectors for these measurements. This causes concern for the analysis of samples whose producer may have tried to conceal the removal of uranium. Cryogenic detectors can remove the line overlap at 186 keV, and thus increase the confidence in the measurements to monitor uranium mining and verify the absence of undeclared activities.

Finally, cryogenic detectors can be used to better attribute natural uranium to a particular source. There are often small differences in isotopic abundances in natural uranium that can serve as fingerprints for the product of a mine or general area of origin. While conventional HPGe detectors sometimes have the sensitivity to detect these differences [18], cryogenic detectors will be able to detect smaller differences with higher accuracy, and thus increase the confidence to assign a illegal shipment to its source.

The current limitation of cryogenic spectrometers that prevents their wider use is their intrinsically small size and low count rate capabilities. Both limitations can be addressed by building detector arrays, which will increase the active area and the maximum count rate by a factor equal to the number of independent channels [5]. Photolithography full-wafer processing allows fabrication of hundreds of identical devices on a single chip, and multiplexing enables the readout of these arrays without excessively increasing the heat load into the spectrometer cold stage [4]. This will be the focus of future research, given that the energy resolution of current cryogenic detectors is already sufficient for most applications in nuclear attribution.

## V. SUMMARY

The Advanced Detector Group at LLNL is developing cryogenic γ-ray spectrometers whose energy resolution of ~50 to 90 eV FWHM below 100 keV exceeds that of conventional HPGe detectors by an order of magnitude. Operation at higher energies is possible with reduced resolution. This can improve the accuracy of non-destructive isotopic ratio measurements by γ–ray spectroscopy by an order of magnitude to ~0.1%, since both statistical and systematic errors can be reduced in cases where the line separation is comparable or less than the spectrometer resolution. This is relevant for measurements of U enrichment and Pu isotopics in the context of nuclear attribution and non-proliferation, since minute differences in composition can provide fingerprints of the sample's age, origin, processing history and intended purpose. Current limitations of cryogenic spectrometers with respect to detection efficiency and total count rate are being addressed by building detector arrays.

## VI. REFERENCES


[1] D. Reilly, N. Ensslin, H. Smith Jr., S. Kreiner, "Passive Non-Destructive Assay of Nuclear Materials", Office of Nuclear Regulatory Research (NUREG CR-5550), Washington, DC, 1991.

[2] For a recent overview of the filed of cryogenic detectors, see the *Proceedings of the 10th International Workshop on Low Temperature Detectors*, LTD-10, edited by F. Gatti, published as *Nuclear Instrumentation and Methods*, vol. A520, 2004.

[3] S. H. Moseley, J. C. Mather, D. McCammon, "Thermal Detectors as X-Ray Spectrometers", *Journal of Applied Physics*, vol. 56, pp. 1257-1262, 1984.

[4] M. F. Cunningham, J. N. Ullom, T. Miyazaki, S. E. Labov, J. Clarke, T. M. Lanting, A. T. Lee, P. L. Richards, J. Yoon, H. Spieler, "High-resolution operation of frequency-multiplexed transition-edge photon sensors", *Applied Physics Letters*, vol. 81, pp. 159-161, 2002.

[5] S. Friedrich, S. F. Terracol, T. Miyazaki, O. B. Drury, Z. A. Ali, M. F. Cunningham, T. R. Niedermayr, T. W. Barbee Jr., J. D. Batteux, S. E. Labov, "Design of a multi-channel ultra-high resolution superconducting gamma-ray spectrometer", accepted for publication in *SPIE Proceedings*, vol. 5540, 2004.

[6] D. T. Chow, M. L. van den Berg, A. Loshak, M. Frank, T. W. Barbee Jr, S. E. Labov, "Gamma-ray spectrometers using superconducting transition edge sensors with active feedback bias", *IEEE Transactions on Applied Superconductivity*, vol. 11, pp. 743-746, 2001.

[7] A. Alessandrello, C. Brofferio, D. V. Camin, O. Cremonesi, A. Giuliani, M. Pavan, G. Pessina, E. Previtali, "An electrothermal model for large mass bolometric detectors", *IEEE Transactions on Nuclear Science,* vol. 40, pp. 649-656, 1993.

[8] T. Miyazaki, in preparation.

[9] K.D. Irwin, "An application of electrothermal feedback for high-resolution cryogenic particle detection", *Applied Physics Letters*, vol. 66, pp. 1998-2000, 1995.

[10] P. L. Ryder, "Theoretical analysis of statistical limitations to the accuracy and spectral resolution in energy-dispersive X-ray analysis", *Scanning Electron Microscopy*, vol. 1, pp. 273-280, 1977.

[11] O. B. Drury, S. F. Terracol, S. Friedrich, "Quantifying the benefits of ultrahigh energy resolution for Gamma-ray spectrometry", accepted for publication to *Physica Status Solidi*, 2005.

[12] R. Gunnink, "MGA: A Gamma-ray spectrum analysis code for determining plutonium isotopic abundances", UCRL-LR-103220, vol. 1, 1990. Available from the National Technical Information Service, U.S. Dept. of Commerce, 5285 Port Royal Rd., Springfield, VA 22161

[13] C. Hagmann, P. L. Richards, "Two-stage magnetic refrigerator for astronomical applications with reservoir temperatures above 4 K", *Cryogenics*, vol. 34, pp. 221-226, 1994.

[14] S. Friedrich, T. Niedermayr, O. B. Drury, M. F. Cunningham, M. L. van den Berg, J. N. Ullom, A. Loshak, T. Funk, S. P. Cramer, J. D. Batteux, E. See, M. Frank, S. E. Labov, "A superconducting detector endstation for high-resolution energy-dispersive SR-XRF", *Nuclear Instrumentation and Methods*, vol. A467, pp. 1117-1120, 2001.

[15] T. Dragnev, V. Rukhlo, D. Rundquist, "Combined Gamma and passive X-ray fluorescence measurement of U-235 enrichment and U-total concentration", *Journal of Radioanalytical Nuclear Chemistry*, vol. 152, pp. 161-173, 1991.

[16] V. Maiorov, M. Ryjinski, V. Bragin, "Detection of uranium mining activities", *Symposium on International Safeguards*, IAEA-SM-367/5/08, Vienna, Austria, 2001.

[17] D. Donohue, V. Maiorov, M. Ryjinski, V. Bragin, B. Frost, "Use of gamma spectrometry for the verification of uranium mining activities", IAEA, 2002.

[18] R. Ovaskainen, K. Mayer, W. De Bolle, D. Donohue, P. De Bievre, "Unusual isotope abundances in natural uranium samples", *ESARDA 19th Annual Symposium on Safeguards and Nuclear Material Management Proceedings,* pp. 293 - 297, 1997.